

Analytical impedance of oxygen transport in the channel and gas diffusion layer of a PEM fuel cell

Andrei Kulikovsky^{a)}

Forschungszentrum Jülich GmbH

Theory and Computation of Energy Materials (IEK-13)

Institute of Energy and Climate Research,

D-52425 Jülich, Germany^{b)}

(Dated: 9 November 2021)

Analytical model for impedance of oxygen transport in the gas-diffusion layer (GDL) and cathode channel of a PEM fuel cell is developed. The model is based on transient oxygen mass conservation equations coupled to the proton current conservation equation in the catalyst layer. Analytical formula for the “GDL+channel” impedance is derived assuming that the oxygen and proton transport in the cathode catalyst layer (CCL) are fast. In the Nyquist plot, the resulting impedance consists of two arcs describing oxygen transport in the air channel (low-frequency arc) and in the GDL. The characteristic frequency of GDL arc depends on the CCL thickness: large CCL thickness strongly lowers this frequency. At small CCL thickness, the high-frequency feature on the arc shape forms. This effect is important for identification of peaks in distribution of relaxation times spectra of low-Pt PEMFCs.

Keywords: PEM fuel cell, impedance, GDL, modeling

I. INTRODUCTION

Electrochemical impedance spectroscopy (EIS) provides invaluable information on transport properties of PEM fuel cell in a current production mode, without interruption of cell functioning¹. Not surprisingly, EIS of PEM fuel cells is a rapidly growing field². Understanding impedance spectra requires modeling. Strong criticism of equivalent circuit approach has been published by Macdonald in his seminal paper³ and in recent years, physics-based models for PEMFC impedance tend to replace equivalent circuit modeling (see recent reviews of Tang et al.² and Huang et al.⁴).

Every transport and kinetic process in a PEM fuel cell has its own resonance frequency. If these frequencies do not overlap, one could identify them using the distribution of relaxation times (DRT) technique⁵⁻⁷. In addition, DRT analysis of impedance spectra returns the contribution of every process into the total differential resistance of the cell. However, correct identification of DRT peaks is a non-trivial task requiring modeling and experimental work. Analytical models predicting characteristic frequencies of oxygen transport processes in the cell could be very helpful in this respect.

Oxygen reduction reaction (ORR) is usually responsible for a large part of potential loss in a PEMFC. Oxygen is transported to the catalyst sites through the cathode channel and gas-diffusion layer; both the transport processes have their signatures in the EIS spectra. After pioneering experimental work of Schneider et al.^{8,9}, Kulikovsky and Shamardina^{10,11}, Maranzana et al.¹² and Chevalier et al.¹³ developed numerical and analytical models incorporating

channel impedance. Formulas for pure channel impedance have been obtained^{13,14} assuming fast oxygen transport through the GDL and cathode catalyst layer (CCL). However, the coupling between the channel and GDL impedance remained poorly understood. Recently, Cruz-Manzo and Greenwood reported analytical model for the GDL+channel impedance¹⁵. However, their result missing important effect of double layer charging on this impedance, as discussed below.

In this work, we develop analytical model for the GDL+channel impedance Z_{gdlc} in a PEM fuel cell. Assuming fast oxygen and proton transport in the CCL, analytical expression for Z_{gdlc} is derived. We show that for typical PEMFC parameters, the Nyquist spectrum of Z_{gdlc} consists of two arcs corresponding to oxygen transport in the channel and GDL. GDL impedance differs from the Warburg finite-length impedance due to “non-Warburg” factor depending on the superficial double layer capacitance of the electrode. For typical PEMFC parameters, the characteristic frequency f_{gdl} of the GDL impedance Z_{gdl} is close to the Warburg finite-length frequency; however, for larger CCL thickness typical for non-Pt cells, the non-Warburg factor strongly lowers f_{gdl} . In the opposite limit of small catalyst layer thickness, a high-frequency feature on the shape of imaginary part of Z_{gdl} vs frequency forms. Analysis shows that the channel impedance also depends on the double layer capacitance meaning that impedance of all oxygen transport medias in the PEMFC “feel” double layer capacitance of the electrode where the oxygen is transported to. The goal of this paper is to clarify the situation with oxygen transport impedance in the GDL and channel after interesting and useful, but incomplete and rather difficult for understanding work of Cruz-Manzo and Greenwood¹⁵.

^{a)}ECS Active member; Electronic mail: A.Kulikovsky@fz-juelich.de

^{b)}Also at: Lomonosov Moscow State University, Research Computing Center, 119991 Moscow, Russia

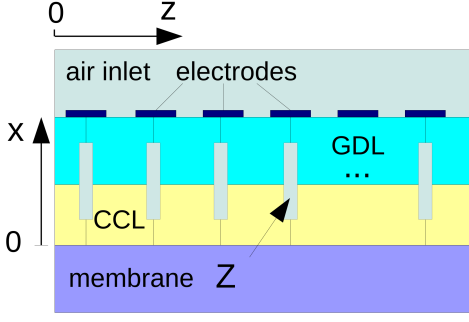


FIG. 1. Schematic of the segmented cell cathode side with the straight channel and the system of coordinates. Z stands for local impedance depending on the distance along the channel coordinate z .

II. MODEL

Schematic of the cell with the straight cathode channel is shown in Figure 1. Our main goal here is analysis of impedance of the GDL+channel oxygen transport system. To simplify the model and to separate the GDL+channel impedance from impedance of oxygen transport in the CCL, we will assume that the latter transport is fast. In addition, for simplicity we will assume that the proton transport in the CCL is also fast. The characteristic frequency of proton transport in the CCL is much higher than the other frequencies in the system and hence this assumption does not affect low- and medium-frequency impedances which are of primary interest in this work.

A. Proton charge conservation equation

The proton charge conservation equation reads

$$C_{dl} \frac{\partial \eta}{\partial t} + \frac{\partial j}{\partial x} = -i_* \left(\frac{c}{c_h^{in}} \right) \exp \left(\frac{\eta}{b} \right) \quad (1)$$

where C_{dl} is the volumetric double layer capacitance (F cm^{-3}), η is the positive by convention ORR overpotential, j is the local proton current density in the CCL, x is coordinate through the cell cathode counted from the membrane, i_* is the volumetric exchange current density (A cm^{-3}), c is the local oxygen concentration, c_h^{in} is the reference oxygen concentration, and b is the ORR Tafel slope.

Since proton and oxygen transport in the CCL are fast, η and c are nearly independent of x . Integrating Eq.(1) over x from 0 to the CCL thickness l_t we come to

$$C_{dl} l_t \frac{\partial \eta_0}{\partial t} - j_0 = -i_* l_t \left(\frac{c_1}{c_h^{in}} \right) \exp \left(\frac{\eta_0}{b} \right) \quad (2)$$

where η_0 is the ORR overpotential at the membrane surface, j_0 is the local cell current density, and c_1 is the oxygen

concentration at the CCL/GDL interface.

To simplify calculations, we introduce dimensionless variables

$$\begin{aligned} \tilde{t} &= \frac{t}{t_*}, & \tilde{x} &= \frac{x}{l_t}, & \tilde{z} &= \frac{z}{L}, & \tilde{c} &= \frac{c}{c_h^{in}}, & \tilde{j} &= \frac{j}{i_* l_t}, \\ \tilde{\eta} &= \frac{\eta}{b}, & \tilde{D}_b &= \frac{4FD_b c_h^{in}}{i_* l_t^2}, & \tilde{l}_b &= \frac{l_b}{l_t}, \\ \tilde{\omega} &= \omega t_*, & \tilde{Z} &= \frac{Z i_* l_t}{b} \end{aligned} \quad (3)$$

where

$$t_* = \frac{C_{dl} b}{i_*}, \quad (4)$$

is the characteristic time of double layer charging, z is the coordinate along the cathode channel, L is the channel length, D_b is the oxygen diffusion coefficient in the GDL, l_b is the GDL thickness, ω is the angular frequency of the applied AC signal, and Z is the local impedance.

With the dimensionless variables (3), Eq.(2) takes the form

$$\frac{\partial \tilde{\eta}_0}{\partial \tilde{t}} - \tilde{j}_0 = -\tilde{c}_1 e^{\tilde{\eta}_0} \quad (5)$$

Substituting Fourier-transforms

$$\begin{aligned} \tilde{\eta}_0 &= \tilde{\eta}_0^0 + \tilde{\eta}_1^1(\tilde{\omega}) \exp(i\tilde{\omega}\tilde{t}) \\ \tilde{j}_0 &= \tilde{j}_0^0 + \tilde{j}_1^1(\tilde{\omega}) \exp(i\tilde{\omega}\tilde{t}) \\ \tilde{c}_1 &= \tilde{c}_1^0 + \tilde{c}_1^1(\tilde{\omega}) \exp(i\tilde{\omega}\tilde{t}) \end{aligned} \quad (6)$$

into Eq.(5), expanding exponent in Taylor series, neglecting term with the perturbations product, and subtracting the static equation, we get equation relating the small perturbation amplitudes $\tilde{\eta}_1^1$, \tilde{j}_1^1 and \tilde{c}_1^1 in the $\tilde{\omega}$ -space:

$$\tilde{j}_1^1 = i\tilde{\omega}\tilde{\eta}_1^1 + e^{\tilde{\eta}_0^0} (\tilde{c}_1^1 + \tilde{c}_1^0 \tilde{\eta}_1^1). \quad (7)$$

Here, the superscripts 0 and 1 mark the static variables and the small perturbation amplitudes, respectively. Local cathode side impedance at a distance \tilde{z} from the channel inlet is given by

$$\tilde{Z} = \frac{\tilde{\eta}_1^1}{\tilde{j}_1^1} \quad (8)$$

Dividing Eq.(7) by \tilde{j}_1^1 , we obtain equation for \tilde{Z} :

$$1 = (i\tilde{\omega} + \tilde{c}_1^0 e^{\tilde{\eta}_0^0}) \tilde{Z} + e^{\tilde{\eta}_0^0} \frac{\tilde{c}_1^1}{\tilde{j}_1^1} \quad (9)$$

Suppose that the perturbation of oxygen concentration is zero: $\tilde{c}_1^1 = 0$. Physically, this is equivalent to fast oxygen transport in all transport medias of the cathode side,

including channel. Solution to Eq.(9) is then

$$\tilde{Z}_f = \frac{1}{i\tilde{\omega} + \tilde{c}_1^0 e^{\tilde{\eta}_0}}, \quad (10)$$

which is impedance of a parallel RC -circuit, where the term $i\tilde{\omega}$ in denominator describes contribution of the double layer capacitance and $\tilde{c}_1^0 e^{\tilde{\eta}_0}$ is the inverse faradaic resistivity of the catalyst layer.

The static oxygen concentration \tilde{c}_1^0 is related to the channel concentration \tilde{c}_h^0 as

$$\tilde{c}_1^0 = \tilde{c}_h^0 \left(1 - \frac{\tilde{j}^0}{\tilde{j}_{\text{lim}}} \right) \quad (11)$$

where

$$j_{\text{lim}} = \frac{4FD_b c_h^0}{l_b} \quad (12)$$

is the local limiting current density due to oxygen transport in the GDL. Eq.(11) is solution of the static version of equation for oxygen transport in the GDL, see Eq.(18) below. The concentration \tilde{c}_h^0 varies along the channel; numerical model¹⁶ shows that unless the mean cell current density is small, this variation to a good approximation is linear:

$$\tilde{c}_h^0 \simeq 1 - \frac{\tilde{z}}{\lambda} \quad (13)$$

Note that Eq.(13) is an approximation¹ the exact shape of $\tilde{c}_h^0(\tilde{z})$ should be calculated using a numerical model^{16,17}.

To simplify calculations, we will ignore the factor $1 - \tilde{j}^0/\tilde{j}_{\text{lim}}$ in Eq.(11), assuming that j_{lim} is large and the variation of static oxygen concentration across the GDL is negligible. With this, Eqs.(7), (9) transform to

$$\tilde{j}^1 = i\tilde{\omega}\tilde{\eta}^1 + e^{\tilde{\eta}_0} \left(\tilde{c}_1^1 + \left(1 - \frac{\tilde{z}}{\lambda} \right) \tilde{\eta}^1 \right) \quad (14)$$

$$1 = \left(i\tilde{\omega} + e^{\tilde{\eta}_0} \left(1 - \frac{\tilde{z}}{\lambda} \right) \right) \tilde{Z} + e^{\tilde{\eta}_0} \frac{\tilde{c}_1^1}{\tilde{j}^1} \quad (15)$$

As discussed above, the non-faradaic oxygen transport contributions to local impedance gives the term with \tilde{c}_1^1 . In order to calculate \tilde{c}_1^1 , we need to consecutively solve equations for oxygen transport in the GDL and channel, as discussed in the next section.

¹ At low cell currents, the shape of local oxygen concentration is exponential¹⁸:

$$\tilde{c}_h^0 = \left(1 - \frac{1}{\lambda} \right)^{\tilde{z}}$$

The model can be reformulated using the above equation for \tilde{c}_h^0 . However, this equation is valid at the low cell currents only, while Eq.(13) works better at higher cell currents, which are of practical interest.

For further references we need a total faradaic impedance $\tilde{Z}_{f,tot}$ of the cathode, taking into account variation of oxygen concentration along the channel. Suppose that the cell is divided into $N \rightarrow \infty$ virtual segments. Local current in each segment flows in the through-plane direction, hence local faradaic impedances are connected in parallel. Thus, $\tilde{Z}_{f,tot}$ is given by

$$\tilde{Z}_{f,tot} = \left(\int_0^1 \frac{d\tilde{z}}{\tilde{Z}_f} \right)^{-1} \quad (16)$$

Electron conductivity of the cell components is assumed to be large and hence $\tilde{\eta}^0$ is independent of the coordinate \tilde{z} . Substituting Eq.(13) into Eq.(10), we get the local faradaic impedance $\tilde{Z}_f(\tilde{z})$. Calculating integral, from Eq.(16) we find

$$\tilde{Z}_{f,tot} = \frac{1}{i\tilde{\omega} + \left(1 - \frac{1}{2\lambda} \right) e^{\tilde{\eta}_0}} \quad (17)$$

B. Oxygen transport in the GDL

Oxygen transport in the gas-diffusion layer is described by the diffusion equation

$$\frac{\partial c_b}{\partial t} - D_b \frac{\partial^2 c_b}{\partial x^2} = 0, \quad D_b \frac{\partial c_b}{\partial x} \Big|_{x=l_t+} = \frac{j_0}{4F},$$

$$c_b(l_t + l_b) = c_h, \quad (18)$$

where c_b is the oxygen concentration in the GDL and c_h is the oxygen concentration in channel. The left boundary condition for Eq.(18) means that the oxygen flux on the GDL side of the CCL/GDL interface equals the local current density in the cell. This condition agrees with the assumption of fast oxygen transport in the CCL.

With the dimensionless variables Eq.(3), Eq.(18) takes the form

$$\mu^2 \frac{\partial \tilde{c}_b}{\partial \tilde{t}} - \tilde{D}_b \frac{\partial^2 \tilde{c}_b}{\partial \tilde{x}^2} = 0, \quad \tilde{D}_b \frac{\partial \tilde{c}_b}{\partial \tilde{x}} \Big|_{\tilde{x}=1+} = \tilde{j}_0,$$

$$\tilde{c}_b(1 + \tilde{l}_b) = \tilde{c}_h, \quad (19)$$

where the dimensionless parameter μ is given by

$$\mu = \sqrt{\frac{4F c_h^{in}}{C_{dl} b}}. \quad (20)$$

Eq.(19) is linear and hence the equation for the small perturbation amplitude \tilde{c}_b^1 is

$$\tilde{D}_b \frac{\partial^2 \tilde{c}_b^1}{\partial \tilde{x}^2} = i\tilde{\omega} \mu^2 \tilde{c}_b^1, \quad \tilde{D}_b \frac{\partial \tilde{c}_b^1}{\partial \tilde{x}} \Big|_{\tilde{x}=1+} = \tilde{j}^1,$$

$$\tilde{c}_b^1(1 + \tilde{l}_b) = \tilde{c}_h^1 \quad (21)$$

where \tilde{c}_h^1 is the oxygen perturbation in channel (see below).

Solution to Eq.(21) is

$$\tilde{c}_b^1 = -\frac{\tilde{j}^1 \sinh\left(\mu\sqrt{i\tilde{\omega}/\tilde{D}_b}(1+\tilde{l}_b-\tilde{x})\right)}{\mu\sqrt{i\tilde{\omega}\tilde{D}_b} \cosh\left(\mu\tilde{l}_b\sqrt{i\tilde{\omega}/\tilde{D}_b}\right)} + \frac{\tilde{c}_h^1 \cosh\left(\mu\sqrt{i\tilde{\omega}/\tilde{D}_b}(1-\tilde{x})\right)}{\cosh\left(\mu\tilde{l}_b\sqrt{i\tilde{\omega}/\tilde{D}_b}\right)} \quad (22)$$

Setting here $\tilde{x} = 1$, we get the perturbation amplitude of oxygen concentration at the CCL/GDL interface $\tilde{c}_b^1(1) = \tilde{c}_1^1$

$$\tilde{c}_1^1 = -\frac{\tilde{j}^1 \tanh(\phi)}{\psi} + \frac{\tilde{c}_h^1}{\cosh(\phi)} \quad (23)$$

where ϕ and ψ are auxiliary dimensionless parameters

$$\begin{aligned} \phi &= \mu\tilde{l}_b\sqrt{i\tilde{\omega}/\tilde{D}_b} \\ \psi &= \mu\sqrt{i\tilde{\omega}\tilde{D}_b} \end{aligned} \quad (24)$$

C. Oxygen transport in channel

To a good approximation, oxygen mass transport in the channel can be described by the 1d + 1d plug flow equation:

$$\frac{\partial c_h}{\partial t} + v \frac{\partial c_h}{\partial z} = -\frac{D_b}{h} \frac{\partial c_b}{\partial x} \Big|_{x=l_t+l_b} \quad (25)$$

where h is the channel depth. The right side of Eq.(25) is the oxygen diffusive flux in the GDL at the channel/GDL interface representing oxygen ‘‘sink’’ from the channel.

With the dimensionless variables (3), Eq.(25) reads

$$\xi^2 \frac{\partial \tilde{c}_h}{\partial \tilde{t}} + \lambda \tilde{J} \frac{\partial \tilde{c}_h}{\partial \tilde{z}} = -\tilde{D}_b \frac{\partial \tilde{c}_b}{\partial \tilde{x}} \Big|_{\tilde{x}=1+\tilde{l}_b} \quad (26)$$

where \tilde{J} is the mean current density in the cell

$$\tilde{J} = \int_0^1 \tilde{j}_0 d\tilde{z}, \quad (27)$$

ξ is the dimensionless parameter, and λ is the stoichiometry of air flow

$$\xi = \sqrt{\frac{4Fhc_h^{in}}{C_{dl}l_t b}}, \quad \lambda = \frac{4Fhvc_h^{in}}{LJ}. \quad (28)$$

Eq.(26) is linear and we can immediately write down

equation for the perturbation amplitude \tilde{c}_h^1 :

$$\lambda \tilde{J} \frac{\partial \tilde{c}_h^1}{\partial \tilde{z}} = -i\tilde{\omega}\xi^2 \tilde{c}_h^1 - \tilde{D}_b \frac{\partial \tilde{c}_b^1}{\partial \tilde{x}} \Big|_{\tilde{x}=1+\tilde{l}_b} \quad (29)$$

Differentiating Eq.(22), we find the flux $\tilde{D}_b \partial \tilde{c}_b^1 / \partial \tilde{x}|_{\tilde{x}=1+\tilde{l}_b}$ and Eq.(29) takes the form

$$\begin{aligned} \lambda \tilde{J} \frac{\partial \tilde{c}_h^1}{\partial \tilde{z}} &= -i\tilde{\omega}\xi^2 \tilde{c}_h^1 - \tilde{j}^1 \cosh(\phi)^{-1} - \tilde{c}_h^1 \psi \tanh(\phi), \\ \tilde{c}_h^1(0) &= 0 \end{aligned} \quad (30)$$

where \tilde{j}^1 is a function of coordinate \tilde{z} and of \tilde{c}_h^1 . To find the explicit dependence $\tilde{j}^1(\tilde{z})$ we substitute (23) into Eq.(14); solving the resulting equation for \tilde{j}^1 we get

$$\begin{aligned} \tilde{j}^1 &= \left(\frac{e^{\tilde{\eta}_0} \tanh(\phi)}{\psi} + 1 \right)^{-1} \\ &\times \left(\left(i\tilde{\omega} + e^{\tilde{\eta}_0} \left(1 - \frac{\tilde{z}}{\lambda} \right) \right) \tilde{\eta}^1 + \frac{e^{\tilde{\eta}_0} \tilde{c}_h^1}{\cosh(\phi)} \right) \end{aligned} \quad (31)$$

D. Solution procedure and total cathode impedance

Substituting \tilde{j}^1 , Eq.(31), into Eq.(30) and solving the resulting equation we find the amplitude of oxygen concentration perturbation along the channel

$$\tilde{c}_h^1(\tilde{z}) = \frac{\tilde{\eta}^1}{B} \left(\left(\frac{A\lambda\tilde{J}}{B} + C \right) \left(\exp\left(\frac{B\tilde{z}}{\lambda\tilde{J}}\right) - 1 \right) - A\tilde{z} \right) \quad (32)$$

where the independent of \tilde{z} coefficients A , B and C are given by

$$A = \frac{\psi e^{\tilde{\eta}_0}}{\lambda \cosh(\phi) (\psi + e^{\tilde{\eta}_0} \tanh(\phi))} \quad (33)$$

$$B = -i\tilde{\omega}\xi^2 - \psi \tanh(\phi) - \frac{\lambda A}{\cosh(\phi)} \quad (34)$$

$$C = -\frac{\psi (i\tilde{\omega} + e^{\tilde{\eta}_0})}{\cosh(\phi) (\psi + e^{\tilde{\eta}_0} \tanh(\phi))} \quad (35)$$

Setting in Eq.(32) $\tilde{\eta}^1 = \tilde{Z}\tilde{j}^1$ and using the result in Eq.(23) we get a formula for \tilde{c}_1^1 , which linearly depends on \tilde{Z} . Substituting this \tilde{c}_1^1 into Eq.(15), we obtain a linear algebraic equation for local impedance \tilde{Z} . Solving this equation, we find local impedance, which includes faradaic and oxygen transport in the channel and GDL processes

$$\tilde{Z}(\tilde{z}) = \frac{B^2}{D_{loc}} \left(\cosh(\phi) + \frac{e^{\tilde{\eta}_0} \sinh(\phi)}{\psi} \right) \quad (36)$$

where

$$D_{loc} = e^{\tilde{\eta}_0} \left(\lambda \tilde{J} A + BC \right) \left(\exp \left(\frac{B \tilde{z}}{\lambda \tilde{J}} \right) - 1 \right) + B^2 \left(i \tilde{\omega} + e^{\tilde{\eta}_0} \left(1 - \frac{\tilde{z}}{\lambda} \right) \right) \cosh(\phi) - e^{\tilde{\eta}_0} B A \tilde{z}. \quad (37)$$

Note that D_{loc} contains complex exponent $\exp \left(B \tilde{z} / (\lambda \tilde{J}) \right)$ leading to oscillations of \tilde{Z} along the channel coordinate \tilde{z} (Ref.¹¹).

The total cathode side impedance is given by

$$\tilde{Z}_{tot} = \left(\int_0^1 \frac{d\tilde{z}}{\tilde{Z}} \right)^{-1} \quad (38)$$

Calculation of integral leads to

$$\tilde{Z}_{tot} = \frac{\lambda B^3}{D_{tot}} \left(\cosh(\phi) + \frac{e^{\tilde{\eta}_0} \sinh(\phi)}{\psi} \right) \quad (39)$$

where

$$D_{tot} = \lambda^2 \tilde{J} e^{\tilde{\eta}_0} \left(\lambda \tilde{J} A + BC \right) \left(\exp \left(\frac{B}{\lambda \tilde{J}} \right) - 1 \right) + \left((i \tilde{\omega} + e^{\tilde{\eta}_0}) \lambda - e^{\tilde{\eta}_0} / 2 \right) B^3 \cosh(\phi) - \lambda e^{\tilde{\eta}_0} B \left(\lambda \tilde{J} A + B(A/2 + C) \right). \quad (40)$$

The closed form of integral in Eq.(38) is a key point leading to analytical formula for \tilde{Z}_{tot} . At high frequencies of the AC signal, \tilde{c}_h^1 and local impedance \tilde{Z} are rapidly oscillating functions of \tilde{z} , which requires a lot of steps in numerical solution of Eq.(29) and makes it difficult numerical calculation of Eq.(38). Analytical result for integral in Eq.(38) solves the problem.

III. RESULTS AND DISCUSSION

Equations of the previous Section contain mean current density in the cell \tilde{J} and the total static potential loss (overpotential) $\tilde{\eta}^0$. These parameters are related by the polarization curve, which could be obtained from solution of the static version of equations (1), (18) and (25). The solution is Tafel-like equation corrected for the finite flow stoichiometry λ (Ref.¹⁹):

$$-\lambda \ln \left(1 - \frac{1}{\lambda} \right) \tilde{J} = e^{\tilde{\eta}_0} \quad (41)$$

Note that Eq.(41) does not include the effect of cell ohmic resistivity. If experimental polarization curve is available, an IR-corrected numerical relation between $\tilde{\eta}^0$ and \tilde{J} could be used instead of Eq.(41). A more accurate numerical approximation for the polarization curve could be obtained using the model^{16,17}.

Eq.(41) allows us to eliminate $e^{\tilde{\eta}_0}$ from Eq.(39). Nyquist

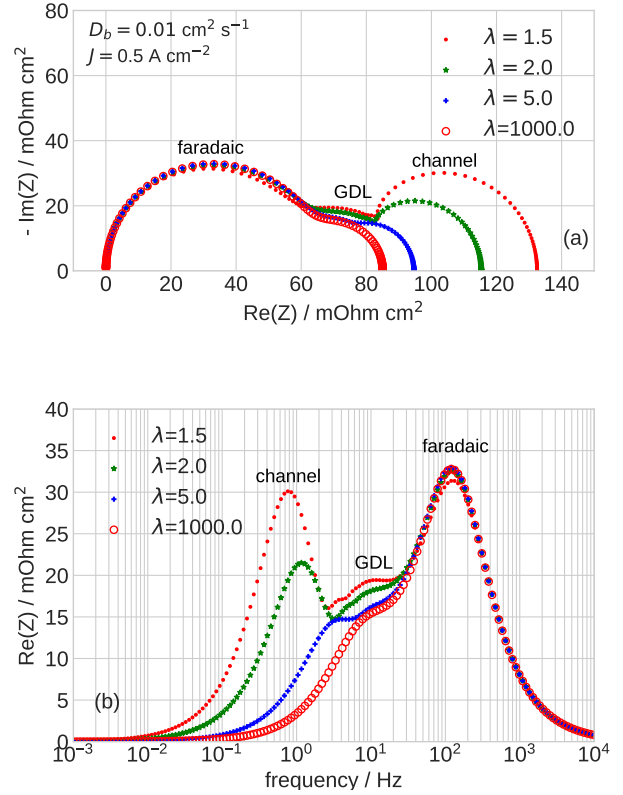


FIG. 2. (a) Nyquist spectra of the total cathode side impedance, Eq.(39), for the indicated air flow stoichiometries λ . The cell current density is 0.5 A cm^{-2} . (b) Frequency dependence of imaginary part of impedance in (a).

spectra of total cathode side impedance Z_{tot} for the parameters listed in Table I, the mean cell current density $J = 0.5 \text{ A cm}^{-2}$ and several stoichiometries of the air flow are shown in Figure 2a. Figure 2b shows the frequency dependence of $\text{Im}(Z_{tot})$. As can be seen, the impedance consists of three arcs, of which the low-frequency (LF) one strongly depends on λ (Figure 2a). In the pioneering experiments of Schneider et al. this arc has been associated with the oxygen transport in channel^{8,9}. The LF arc vanishes as $\lambda \rightarrow \infty$ (Figures 2a,b).

The medium-frequency (MF) arc in Figure 2a represents oxygen transport in the GDL. This arc is not fully seen due to masking effect of the third, high-frequency (HF) faradaic arc (Figure 2). To emphasize the GDL arc, we subtract the total faradaic impedance (17) from the total cathode impedance, Eq.(39). This leads to the GDL+channel impedance \tilde{Z}_{gdlc} :

$$\tilde{Z}_{gdlc} = \tilde{Z}_{tot} - \frac{1}{i \tilde{\omega} + \left(1 - \frac{1}{2\lambda} \right) e^{\tilde{\eta}_0}} \quad (42)$$

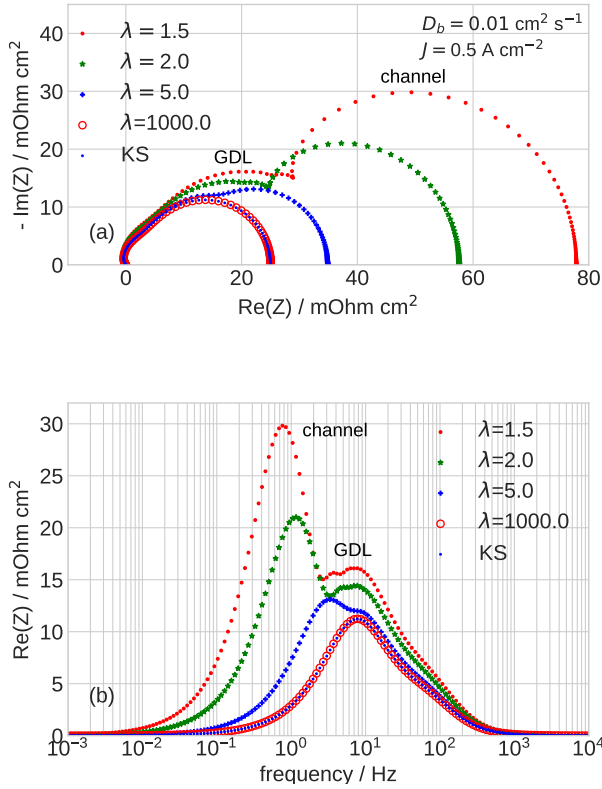


FIG. 3. (a) Nyquist spectra of the GDL+channel impedance, Eq.(42) for the indicated air flow stoichiometries λ . The cell current density is $J = 0.5 \text{ A cm}^{-2}$. KS marks the spectrum of Eq.(44). (b) Frequency dependence of imaginary part of impedance in (a).

Nyquist spectra of Eq.(42) for the same parameters exhibit two arcs; now the left, GDL arc is fully resolved (Figure 3a). Frequency dependence of $\text{Im}(Z_{gdlc})$ is shown in Figure 3b. Two peaks in Figure 3b correspond to the channel and GDL arcs in Figure 3a. At low stoichiometry of the air flow, the GDL arc is located at the right “wing” of the channel arc; the latter contributes to imaginary part of the GDL impedance (Figure 3b). However, as λ increases, the channel arc vanishes and only GDL arc is left (the curves for $\lambda = 1000$ in Figures 3a,b).

Equation for GDL impedance in the limit of infinite air flow stoichiometry has been derived by Kulikovskiy and Shamardina¹¹. In the notations of this work, Eq.(36) of Ref.¹¹ is

$$\tilde{Z}_{gdl} = \frac{\tanh\left(\mu\tilde{l}_b\sqrt{i\tilde{\omega}/\tilde{D}_b}\right)}{\mu\sqrt{i\tilde{\omega}\tilde{D}_b}\left(1 - \tilde{J}\tilde{l}_b/\tilde{D}_b\right)\left(1 + i\tilde{\omega}/\tilde{J}\right)} \quad (43)$$

The frequency-independent factor $(1 - \tilde{J}\tilde{l}_b/\tilde{D}_b)$ in denominator describes the growth of static resistivity upon ap-

GDL thickness l_b , cm	0.023
Catalyst layer thickness l_t , cm	$10 \cdot 10^{-4}$ (10 μm)
ORR Tafel slope b , mV	30
Double layer capacitance C_{dl} , F cm^{-3}	20
GDL oxygen diffusivity D_b , $\text{cm}^2 \text{s}^{-1}$	0.01
Cell current density j_0 , A cm^{-2}	0.1
Pressure	Standard
Cell temperature T , K	273 + 80
Air flow stoichiometry λ	2.0

TABLE I. The base-case cell parameters used in calculations.

proaching the limiting current density \tilde{D}_b/\tilde{l}_b due to oxygen transport in the GDL. In this work, we assume that the limiting current is large and the factor $(1 - \tilde{J}\tilde{l}_b/\tilde{D}_b)$ can be replaced by unity. With this, Eq.(43) simplifies to

$$\tilde{Z}_{gdl} = \frac{\tanh\left(\mu\tilde{l}_b\sqrt{i\tilde{\omega}/\tilde{D}_b}\right)}{\mu\sqrt{i\tilde{\omega}\tilde{D}_b}\left(1 + i\tilde{\omega}/\tilde{J}\right)} \quad (44)$$

Eq.(44) can be directly obtained from Eq.(42) by passing to the limit $\lambda \rightarrow \infty$. The spectrum of Eq.(44) (KS-spectrum) is shown in Figures 3a,b by small blue dots. As expected, the spectrum of Eq.(42) for $\lambda = 1000$ (red open circles, Figure 3a,b) is practically indistinguishable with the spectrum of Eq.(44).

Of particular interest is the “non-Warburg” factor $(1 + i\tilde{\omega}/\tilde{J})$ in denominator of Eq.(44). Without this factor, Eq.(44) is equivalent to the Warburg finite-length impedance¹. “Non-Warburg” shape of the GDL Nyquist arc (HF part of this arc looks like an elephant’s trunk, Figure 3a) is due to the effect of charging double layer capacitance in the CCL¹¹. In other words, the GDL impedance “feels” the double layer capacitance of the attached CCL, since CCL provides a boundary condition for oxygen transport through the GDL. Similar capacitive correction to the classic Warburg impedance has been discussed by Barbero²⁰ in the context of Poisson-Nernst-Planck model for the planar electrode. It is worth noting a detailed study of the effect of non-capacitive boundary conditions on Warburg impedance published recently by Huang²¹.

The non-Warburg factor $(1 + i\tilde{\omega}/\tilde{J})$ in Eq.(44) leads to important effects. In the dimension form, $i\tilde{\omega}/\tilde{J} = i\omega C_{dl}l_t b/J$, i.e., this factor includes the superficial double layer capacitance $C_{dl}l_t$ (F cm^{-2}) of the CCL. Under constant volumetric DL capacitance C_{dl} (F cm^{-3}), this results in dependence of the GDL spectrum on the catalyst layer thickness l_t . Figure 4 shows that with typical for Pt/C-based PEMFCs CCL thickness in the range of 10 μm to 1 μm , the effect of non-Warburg factor on the characteristic frequency f_{gdl} of GDL spectrum is small and f_{gdl} is close to the Warburg finite-length frequency f_W :

$$f_W = \frac{2.54D_b}{2\pi l_b^2} \quad (45)$$

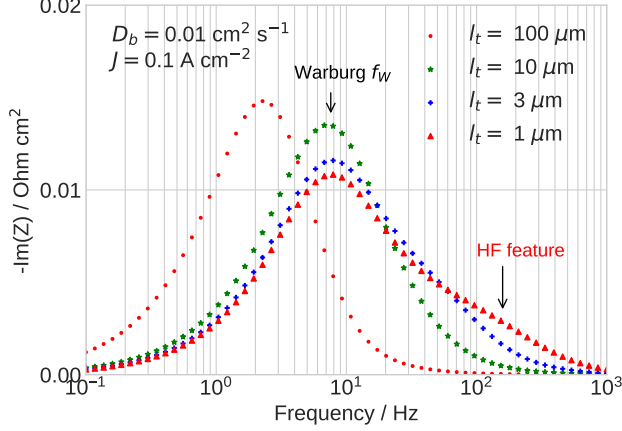


FIG. 4. Frequency dependence of imaginary part of the GDL impedance, Eq.(44), for the indicated values of CCL thickness l_t . The cell current density is 0.1 A cm^{-2} . The volumetric double layer capacitance C_{dl} is assumed to be constant for all the curves.

However, for CCL thickness on the order of $100 \mu\text{m}$ typical for cells with non-Pt catalysts²², the non-Warburg factor strongly shifts the frequency f_{gdl} to lower values (Figure 4). This may lead to partial overlapping of the GDL and channel peaks of the respective imaginary parts (cf. Figure 3b, the curve for $\lambda = 5$). Figure 4 also shows that with the decrease in CCL thickness, the width of the GDL peak increases. Moreover, at low l_t , the non-Warburg factor leads to formation of a distinct high-frequency feature in the spectrum (Figure 4). The effects in Figure 4 are particularly important for identification of DRT peaks in the high- and low-Pt PEM fuel cell spectra. The thickness of a low-Pt CCL is typically three to four times less than the high-Pt CCL thickness, while the volumetric C_{dl} in both types of cells is the same.

Finally, a formula for “pure” channel impedance \tilde{Z}_{chan} can be obtained from Eqs.(42), (39) by setting GDL thickness to zero:

$$\tilde{Z}_{chan} = -\frac{4\lambda e^{\tilde{\eta}_0} N_c}{(2\lambda i\tilde{\omega} + (2\lambda - 1)e^{\tilde{\eta}_0}) D_c} \quad (46)$$

where N_c and D_c are given in Appendix. The characteristic frequency f_{chan} of channel impedance depends almost linearly of the cell current density and on the air flow stoichiometry (Figure 5). It is interesting to note that the slope of $f_{chan}(J)$ increases with the growth of stoichiometry λ (Figure 5a), although the magnitude of \tilde{Z}_{chan} rapidly decreases with λ .

Setting in Eq.(46) $\tilde{\omega} = 0$, we find the static resistivity

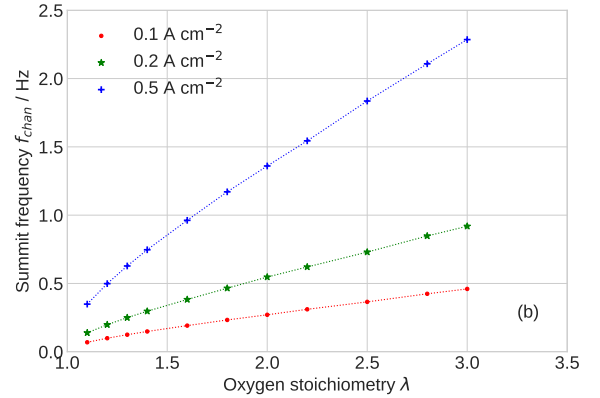
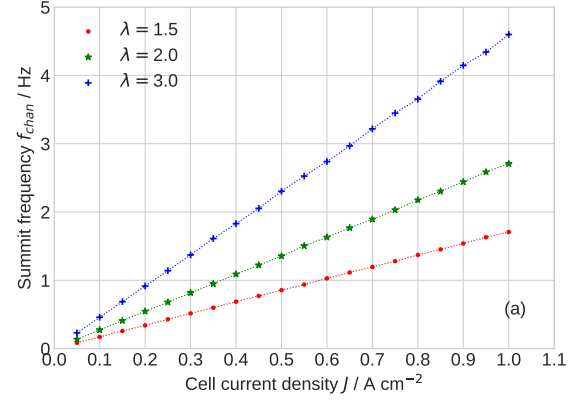


FIG. 5. (a) The characteristic frequency of channel impedance f_{chan} vs cell current density for the indicated air flow stoichiometries. (b) The frequency f_{chan} vs air flow stoichiometry for the indicated cell current densities.

due to channel; in the dimension form this resistivity reads

$$R_{chan} = \frac{b}{J} \left(\frac{2}{(2\lambda - 1) \ln(1 - 1/\lambda)} - \lambda \ln \left(1 - \frac{1}{\lambda} \right) \right) \quad (47)$$

Eq.(47) is independent of parameter ξ , Eq.(28); however, ξ affects the shape of impedance (46). As ξ contains the product $C_{dl}l_t$, the shape of \tilde{Z}_{chan} appears to be dependent of the CCL thickness. Though for typical PEMFC parameters this dependence is weak, we should stress that impedance of oxygen transport layers (GDL and channel) depend on the double layer capacitance in the electrode.

IV. CONCLUSIONS

An analytical model for impedance of oxygen transport in the GDL and channel of a PEM fuel cell cathode is developed. The model is based on 1d+1d-coupled oxygen mass transport equations along the channel and through the GDL. The oxygen and proton transport through the cathode catalyst layer are assumed to be fast. Analytical solution for the

GDL+channel impedance Z_{gdlc} is obtained. The Nyquist spectrum of Z_{gdlc} consists of two arcs, of which the left arcs corresponds to oxygen transport in the GDL and the right (LF) arc is due to oxygen transport in the channel. The characteristic frequency of the channel arc depends linearly on the oxygen stoichiometry. The shape of the GDL arc differs from the Warburg finite-length impedance due to effect of double layer charging in the catalyst layer attached to the GDL. For typical PEMFC parameters, the characteristic frequency of the GDL arc f_{gdl} is close to the Warburg finite-length frequency. However, for larger CCL thickness the non-Warburg factor strongly shifts f_{gdl} to lower values. At low catalyst layer thickness, the high-frequency feature in the spectrum of imaginary part of the GDL impedance forms. This effect is particularly important for identification of DRT peaks in low-Pt cell spectra, as low-Pt cells typically differ from the high-Pt cells by the catalyst layer thickness only.

Appendix A: Equations for the factors N_c and D_c in Eq.(46)

$$N_c = \lambda^2 \tilde{J} \left(e^{2\tilde{\eta}_0} + \left(\tilde{J} + i\tilde{\omega}(1 + \xi^2) \right) e^{\tilde{\eta}_0} - \xi^2 \tilde{\omega}^2 \right) \times \exp \left(\frac{-e^{\tilde{\eta}_0} - i\tilde{\omega}\xi^2}{\lambda\tilde{J}} \right) + \lambda \left(e^{\tilde{\eta}_0} - \lambda\tilde{J} + i\tilde{\omega}\xi^2 \right) \times \left(e^{2\tilde{\eta}_0} + \left(\tilde{J} + i\tilde{\omega}(\xi^2 + 1) \right) e^{\tilde{\eta}_0} - \xi^2 \tilde{\omega}^2 \right) - \left(e^{\tilde{\eta}_0} + i\tilde{\omega}\xi^2 \right)^2 e^{\tilde{\eta}_0} / 2 \quad (A1)$$

$$D_c = 2\lambda^2 \tilde{J} \left(e^{2\tilde{\eta}_0} + \left(\tilde{J} + i\tilde{\omega}(1 + \xi^2) \right) e^{\tilde{\eta}_0} - \xi^2 \tilde{\omega}^2 \right) \times \exp \left(\frac{-e^{\tilde{\eta}_0} - i\tilde{\omega}\xi^2}{\lambda\tilde{J}} \right) e^{\tilde{\eta}_0} - 2\lambda\xi^6 \tilde{\omega}^4 + i \left(2\lambda\xi^2 - \xi^2 + 4\lambda \right) \xi^4 e^{\tilde{\eta}_0} \tilde{\omega}^3 + 2\xi^2 \left((2\lambda\xi^2 - \xi^2 + \lambda) e^{\tilde{\eta}_0} + \lambda^2 \tilde{J} \right) e^{\tilde{\eta}_0} \tilde{\omega}^2 - i \left((2\lambda - 1) \xi^2 e^{\tilde{\eta}_0} + 2\lambda\tilde{J} (\lambda\xi^2 - \xi^2 + \lambda) \right) e^{2\tilde{\eta}_0} \tilde{\omega} - 2\lambda\tilde{J} \left((\lambda - 1) e^{\tilde{\eta}_0} + \lambda\tilde{J} \right) e^{2\tilde{\eta}_0} \quad (A2)$$

¹A. Lasia. *Electrochemical Impedance Spectroscopy and its Applications*. Springer, New York, 2014.

²Zh. Tang, Q.-A. Huang, Y.-J. Wang, F. Zhang, W. Li, A. Li, L. Zhang, and JJ Zhang. Recent progress in the use of electrochemical impedance spectroscopy for the measurement, monitoring, diagnosis and optimization of proton exchange membrane fuel cell performance. *J. Power Sources*, 468:228361, 2020. doi:10.1016/j.jpowsour.2020.228361.

³D. Macdonald. Reflections on the history of electrochemical impedance spectroscopy. *Electrochim. Acta*, 51:1376–1388, 2006. doi:10.1016/j.electacta.2005.02.107.

⁴J. Huang, Y. Gao, J. Luo, S. Wang, C. Li, S. Chen, and J. Zhang. Editors' choice-review-impedance response of porous electrodes:

- Theoretical framework, physical models and applications. *J. Electrochem. Soc.*, 167:166503, 2020. doi:10.1149/1945-7111/abc655.
- ⁵R.M. Fuoss and J.G. Kirkwood. Electrical properties of solids. viii. Dipole moments in polyvinyl chloride-diphenyl systems. *J. Am. Chem. Soc.*, 63:385–394, 1941. doi:10.1021/ja01847a013.
- ⁶H. Schichlein, A. C. Müller, M. Voigts, A. Krügel, and E. Ivers-Tiffée. Deconvolution of electrochemical impedance spectra for the identification of electrode reaction mechanisms in solid oxide fuel cells. *J. Appl. Electrochem.*, 32:875–882, 2002. doi:10.1023/A:1020599525160.
- ⁷S. Effendy, J. Song, and M. Z. Bazant. Analysis, design, and generalization of electrochemical impedance spectroscopy (EIS) inversion algorithms. *J. Electrochem. Soc.*, 167:106508, 2020. doi:10.1149/1945-7111/ab9c82.
- ⁸I. A. Schneider, S. A. Freunberger, D. Kramer, A. Wokaun, and G. G. Scherer. Oscillations in gas channels. Part I. The forgotten player in impedance spectroscopy in PEFCs. *J. Electrochem. Soc.*, 154:B383–B388, 2007. doi:10.1149/1.2435706.
- ⁹I. A. Schneider, D. Kramer, A. Wokaun, and G. G. Scherer. Oscillations in gas channels. II. Unraveling the characteristics of the low-frequency loop in air-fed PEFC impedance spectra. *J. Electrochem. Soc.*, 154:B770–B782, 2007. doi:10.1149/1.2742291.
- ¹⁰A. A. Kulikovskiy. A model for local impedance of the cathode side of PEM fuel cell with segmented electrodes. *J. Electrochem. Soc.*, 159:F294–F300, 2012. doi:10.1149/2.066207jes.
- ¹¹A. Kulikovskiy and O. Shamardina. A model for PEM fuel cell impedance: Oxygen flow in the channel triggers spatial and frequency oscillations of the local impedance. *J. Electrochem. Soc.*, 162:F1068–F1077, 2015. doi:10.1149/2.0911509jes.
- ¹²G. Maranzana, J. Mainka, O. Lottin, J. Dillet, A. Lamibrac, A. Thomas, and S. Didierjean. A proton exchange membrane fuel cell impedance model taking into account convection along the air channel: On the bias between the low frequency limit of the impedance and the slope of the polarization curve. *Electrochim. Acta*, 83:13–27, 2012.
- ¹³S. Chevalier, C. Josset, A. Bazylak, and B. Auvity. Measurements of air velocities in polymer electrolyte membrane fuel cell channels using electrochemical impedance spectroscopy. *J. Electrochem. Soc.*, 163:F816–F823, 2016. doi:10.1149/2.0481608jes.
- ¹⁴A. Kulikovskiy. Analytical impedance of oxygen transport in a PEM fuel cell channel. *J. Electrochem. Soc.*, 166:F306–F311, 2019. doi:10.1149/2.0951904jes.
- ¹⁵S. Cruz-Manzo and P. Greenwood. Analytical Warburg impedance model for EIS analysis of the gas diffusion layer with oxygen depletion in the air channel of a PEMFC. *J. Electrochem. Soc.*, 168:074502, 2021. doi:10.1149/1945-7111/ac1031.
- ¹⁶T. Reshetenko and A. Kulikovskiy. On the distribution of local current density along the PEM fuel cell cathode channel. *Electrochem. Comm.*, 101:35–38, 2019. doi:10.1016/j.elecom.2019.02.005.
- ¹⁷S. Chevalier, C. Josset, and B. Auvity. Analytical solutions and dimensional analysis of pseudo 2D current density distribution model in PEM fuel cells. *Renew. Energy*, 125:738–746, 2018. doi:10.1016/j.renene.2018.02.120.
- ¹⁸A. A. Kulikovskiy. The voltage current curve of a PEM fuel cell: Analytical and numerical modeling. In M. Laudon and B. Romanowicz, editors, *Techn. Proc. of the 2003 Nanotechnology Conf. and Trade Show*, volume 3, pages 467–470, San-Francisco, CA, USA, February 23–27 2003. Computational Publications.
- ¹⁹A. A. Kulikovskiy. The effect of stoichiometric ratio λ on the performance of a polymer electrolyte fuel cell. *Electrochim. Acta*, 49(4):617–625, 2004.
- ²⁰G. Barbero. Warburg's impedance revisited. *Phys. Chem. Chem. Phys.*, 18:29537–29542, 2016. doi:10.1039/c6cp05049b.
- ²¹J. Huang. Diffusion impedance of electroactive materials, electrolytic solutions and porous electrodes: Warburg impedance and beyond. *Electrochim. Acta*, 281:170–188, 2018. doi:10.1016/j.electacta.2018.05.136.
- ²²T. Reshetenko, G. Randolph, M. Odgaard, B. Zulevi, A. Serov, and A. Kulikovskiy. The effect of proton conductivity of Fe-N-C-based cathode on PEM fuel cell performance. *J. Electrochem. Soc.*, 167:

Nomenclature

\sim	Marks dimensionless variables
b	ORR Tafel slope, V
C_{dl}	Double layer volumetric capacitance, F cm ⁻³
c_1	Oxygen molar concentration at the CCL/GDL interface, mol cm ⁻³
c_b	Oxygen molar concentration in the GDL, mol cm ⁻³
c_h	Oxygen molar concentration in the channel, mol cm ⁻³
c_h^{in}	Reference (inlet) oxygen concentration, mol cm ⁻³
D_b	Oxygen diffusion coefficient in the GDL, cm ² s ⁻¹
F	Faraday constant, C mol ⁻¹
f	Characteristic frequency, Hz
i_*	ORR volumetric exchange current density, A cm ⁻³
i	Imaginary unit
j	Local proton current density along the CCL, A cm ⁻²
j_{lim}	Limiting current density due to oxygen transport in the GDL, Eq.(12) A cm ⁻²
j_0	Local cell current density, A cm ⁻²
l_b	GDL thickness, cm
l_t	CCL thickness, cm
t	Time, s
t_*	Characteristic time, s, Eq.(4)
x	Coordinate through the cell, cm
Z	Local impedance, Ohm cm ²
Z_{gdlc}	GDL+channel impedance, Ohm cm ²
Z_{tot}	Total cathode side impedance, including faradaic one, Ohm cm ²
z	Coordinate along the cathode channel, cm

Subscripts:

0	Membrane/CCL interface
1	CCL/GDL interface
b	In the GDL
gdl	GDL
$gdlc$	GDL+channel
f	faradaic
h	Air channel
W	Warburg

Superscripts:

0	Steady-state value
1	Small-amplitude perturbation

Greek:

η	ORR overpotential, positive by convention, V
λ	Air flow stoichiometry, Eq.(28)
μ	Dimensionless parameter, Eq.(20)
ξ	Dimensionless parameter, Eq.(28)
ϕ	Dimensionless parameter. Eq.(24)
ψ	Dimensionless parameter. Eq.(24)
ω	Angular frequency of the AC signal, s ⁻¹